inventions

MDPI

Article

Hydraulic Design of an Ultracompact Liquid Methane–Liquid Oxygen Turbopump for a Mid-Scale Thruster for Upper Stage Application

Alexandru-Claudiu Cancescu [1,2,*], Daniel-Eugeniu Crunteanu [2], Anna-Maria Theodora Andreescu [3], Simona-Nicoleta Danescu [3] and Valeriu Dragan [3]

[1] R&D Launchers and In-Space Advanced Propulsion System Department, National Research and Development Institute for Gas Turbines COMOTI, 061126 Bucharest, Romania
[2] Doctoral School of Aerospatial Engineering, National University of Science and Technology Politehnica of Bucharest, 060042 Bucharest, Romania; daniel.crunteanu@upb.ro
[3] National Research and Development Institute for Gas Turbines COMOTI, 061126 Bucharest, Romania; theodora.andreescu@comoti.ro (A.-M.T.A.); simona.danescu@comoti.ro (S.-N.D.); valeriu.dragan@comoti.ro (V.D.)
* Correspondence: alexandru.cancescu@comoti.ro

Abstract: As space missions proliferate and the payload requirements increase, the environmental impact of thrusters can no longer be considered negligible. Therefore, less impactful fuels such as methane are starting to be considered for launchers. In this paper we present a design case study for such a turbopump. Using both analytical models and Computational Fluid Dynamics techniques, we were able to reduce the size and weight of the turbopump assembly. Also, due to the elimination of some auxiliary systems, the overall efficiency was enhanced. This paper's findings and methods can be transferred not only to launchers in its own class, but also to larger scale engines with a similar construction.

Keywords: green propulsion; turbopump; methalox; upper stage; mid-scale thruster

Citation: Cancescu, A.-C.; Crunteanu, D.-E.; Andreescu, A.-M.T.; Danescu, S.-N.; Dragan, V. Hydraulic Design of an Ultracompact Liquid Methane–Liquid Oxygen Turbopump for a Mid-Scale Thruster for Upper Stage Application. *Inventions* **2024**, *9*, 104. https://doi.org/10.3390/inventions9050104

Academic Editors: Umberto Lucia, Debora Fino and Giulia Grisolia

Received: 9 August 2024
Revised: 15 September 2024
Accepted: 20 September 2024
Published: 25 September 2024

1. Introduction

Among other measures taken to reduce the costs per launch and the pollution generated, substances such as methane have been considered. Methane has advantages such as a high energy density, a low carbon-to-hydrogen ratio (the smallest among all hydrocarbons), a storage temperature close to the one of oxygen and it is available in nature.

Methane is second in the list of greenhouse effect substances generated by human activity, being 28-times more potent than carbon dioxide at retaining heat [1]. For each molecule of methane that is burnt, one molecule of carbon dioxide and two molecules of water are formed. For this reason, it can be concluded that using methane as fuel (and consequently removing it from the atmosphere) is beneficial to nature.

Engines that use LCH4/LOX as propellants are:

TQ-12 [2]

TQ-12 is an engine developed by LandScape which uses the gas-generator cycle and produces 658 kN of thrust at sea level. Its specific impulse is 337 s. The first successful flight of a rocket using this engine took place in July 2023 (the Zhuque-2 rocket).

BE-4 [3]

BE-4 is an engine developed by Blue Origin which uses the staged combustion cycle and produces 2450 kN of thrust at sea level. The first successful flight of a rocket using this engine took place in January 2024 (the Vulcan Centaur rocket).

Raptor [4]

Raptor is a family of engines developed by SpaceX which use the full-flow staged combustion cycle and produce 1800 kN (Raptor 1)–2750 kN (Raptor 3) of thrust at sea level. Its first low-altitude test flights were performed in 2019 (the Starhopper test vehicle).

M10 [5]

M10 is an engine developed by AVIO for VEGA-E and VEGA-E Light upper stages. It is a derivation of the RD-0146 Russian engine. It uses the expander cycle and has a thrust of 98 kN. It is under development, its first series of testing ending in July 2022. M10 is Europe's first operational methalox engine.

To increase the efficiency of the combustion, the propellants must be inserted in the thrust chamber at a certain pressure, which is higher than the one of the surrounding medium. This pressure can be achieved by means of a pressurized tank, which is applicable only to very small thrusters due to the weight induced by the needed increase in tank walls' thickness or by means of a pumping system.

The pumping system is formed by a pump for each propellant and a system to provide power to the pumps. Depending on the actual construction of the system, the power is provided by means of turbines or electric motors.

In the case of the propulsion system for which the turbopump in this paper is designed, the design cycle is expander cycle. In this cycle, the pumps are powered by means of turbines which use as a working fluid one (or both) of the propellants. The propellant, after leaving the pump, is inserted in the cooling channels of the thrust chamber, where it is heated while cooling the chamber. This heated propellant is then introduced in the turbine, which extracts a part of its energy and transfers it to the pump. Finally, the propellant leaving the turbine is injected in the thrust chamber and burned.

The rocket turbopump systems which use only one turbine to power both pumps have two possible constructions. The first construction type is the one where there are two shafts connected by a gearbox, while the second type is the single-shaft construction. Both types have been used in past turbopump assemblies. Using a gearbox between the shafts in the first construction's case makes it possible for each pump to work at its optimal rotation speed, but the gearbox adds complexity, weight and losses to the system. Single-shaft turbopump systems are less complex, weigh less and have a better efficiency compared to the two-shaft counterpart but impose the same rotation speed on the pumps and turbine.

Y. Demyanenko et al. [6] present a short history of the evolution of turbopump assemblies developed by Russian institute KBKhA. Turbopumps of Russian-developed engines use the single-shaft construction, apart from the RD-0146, which uses a double-shaft construction. The institute used the expertise gained during the development of RD-0120 and RD-0146 to develop a single-shaft turbopump for the RL10 engine.

RL10 was the first expander cycle developed by Pratt & Whitney Rocketdyne. Its original turbopump was built using the construction with two shafts connected to a single turbine through a gearbox. A single-shaft alternative turbopump is proposed. This alternative used a booster pump for liquid oxygen. The booster pump is powered by liquid oxygen taken from the outlet of the main oxygen pump and is based on KBKhA design8.

The turbopump design consists of a dual inlet, back-to-back impeller oxygen pump, which is fed through a volute, a two-stage axial turbine in the middle and a two-stage hydrogen pump.

By implementing this constructive solution, the thrust of the engine is increased by up to 40%, according to the authors.

P. Pempie and H. Vernin [7] present the advantages of using the liquid methane for powering rocket engines. They compare three constructive variants of the LE-5 engine: the gas generator cycle variant (LE-5), the hot bleed cycle variant (LE-5A) and the cold bleed (LE-5B) variant, respectively. The cold bleed cycle uses fluid taken from the cooling system of the nozzle, while in the case of the hot bleed cycle the fluid is passed through a second cooling system where it is heated even further. The cold cycle provides the highest thrust, but it has a slightly lower specific impulse due to the need to use a higher percentage of the

fuel to power the turbine comparable to the other variants, where the gas powering the turbine has a higher temperature.

They present the constructive solutions chosen for the design of a 250 kN engine for the first stage of a reusable launcher. The combustion chamber and a single-shaft turbopump design are then presented.

The turbopump consists of a single-stage oxygen pump, a single-stage methane pump in the middle and a two-stage axial turbine. The authors then present two variants of launchers based on this engine design: a nano launcher capable of placing 100 kg on a sun-synchronous orbit, and an 1000 kN launcher using four of the presented engines, which use a common turbopump to provide the needed propellants to all of them.

The two papers present a single-shaft variant for turbopumps of rocket engines. They both have in common the fact that the turbine uses a multi-stage axial design, and in both cases one of the pumps' inlet is connected directly to the inlet pipe.

Furthermore, the turbopumps of the rocket engines in operation use axial turbines to power the pumps.

A. Leto and A. Bonfiglioli [8] present the RTGD software (https://www.sciencedirect.com/science/article/pii/S187661021733727X, accessed on 5 August 2024) developed by CIRA (Italian Center for Aerospace Research) in HYPROB, which has the scope to develop competences in the radial turbine domain, to introduce them in the design of future rocket engines.

They presented three control tests: a verification against RL10A-3-3A comparing the results with the ones provided by ROCETS, a similar tool developed by NASA, a verification against Vinci, where the results have been compared with the experimental results and, lastly, RPA (Rocket Propulsion Analysis) is used to guess the missing data for the LM10-MIRA turbopump.

Although the model used by RTGD is a simple low-dimensional model, it indicates that there is an interest for a future radial turbine design. Radial turbines are more compact and present a high reliability. Their performances are good even in unsteady flows and their costs are low.

The main goal of the design process for the turbopump was to obtain a compact system, which, as much as possible, does not need auxiliary systems for its operation.

The auxiliary systems considered for elimination are the sealing systems that use the flow of separation liquids or gases and the cooling system of the bearings.

To achieve the goal, a special arrangement of the turbine and pumps has been proposed, which reduces the pressure differences between the adjacent components. These reduced differences allowed the simplification of the sealing system, while also maintaining the operational safeness.

The second design direction was to find and use a bearing system that could accommodate the loads induced by the operation of the turbopump while requiring a minimal amount of lubrication.

This second goal was also facilitated by the design mentioned above since the chosen arrangement lowers the resultant forces in the shaft. By scanning the available bearing systems market, we were able to identify off-the-shelf bearings, which are capable of sustaining the loads and angular velocities of the turbopump.

Weight reduction measures have also been taken, resulting in a turbopump which weighs less than 11 kg, out of which the turbopump assembly weighs less than 6 kg, the rest being the union nuts used as attachment means.

2. Materials and Methods

2.1. Input Conditions

The rocket engine for which the turbopump in this paper is designed is a 30 kN engine. It was designed by the Romanian Research & Development Institute for Gas Turbines COMOTI in the TURBOPROP "Nucleu" Program. The parametric investigation of this case

study is presented in paper [9]. An alternative design which is not focused on the reduction in dimensions or auxiliary systems of the turbopump components is also presented.

The mass flow and chamber pressure have been taken from this article, while the pressure of the propellants found in the tanks has been imposed based on the experience of the authors in other projects.

By calculating the injectors needed for the injection of the propellants in the combustion chamber of the engine using the mathematical model in chapter 8.1 (p. 276) of book [10], the pressure lost by the propellants passing through them can be determined. By adding this value to the required chamber pressure, the oxygen pressure at the outlet from the oxygen pump and the methane pressure at the outlet from the turbine are defined.

The inlet pressure has been calculated using the Darcy–Weisbach equation based on a preliminary design pressure of 4.5 bar of fluid in each tank. The Darcy friction factor formula used in the calculation is the one of Churchill (1973).

$$\Delta p_{loss} = \frac{1}{2} f \rho v^2 \frac{L_h}{D} \tag{1}$$

where:

Δp_{loss}—pressure losses in the lines between the propellant tank and the inlet of the pump.

f—Darcy friction factor.

The Darcy friction factor formula used in the calculation is the one of Churchill (1977) due to its applicability on all flow regimes.

$$f = 8\left[\left(\frac{8}{Re}\right)^{12} + \frac{1}{(\Theta_1 + \Theta_2)^{1.5}}\right]^{\frac{1}{12}} \tag{2}$$

$$\Theta_1 = \left\{-2.457 ln\left[\left(\frac{7}{Re}\right)^{0.9} + 0.27\frac{\varepsilon}{D}\right]\right\}^{16} \tag{3}$$

$$\Theta_2 = \left(\frac{37530}{Re}\right)^{16} \tag{4}$$

Re—Reynolds number of the flow.

$$Re = \frac{\rho v D}{\mu} \tag{5}$$

ρ—density of the propellant.

v—velocity of the propellant, calculated using the mass flow formula.

$$v = \frac{4\dot{m}}{\pi D^2 \rho} \tag{6}$$

$\dot{m}$—mass flow of propellant.

D—hydraulic diameter of the lines.

μ—dynamic viscosity of the propellant.

ε—roughness of the lines.

L_h—(hydraulic) length of the lines.

To design the three components of the ultracompact turbopump, a target rotation speed of 60,000 rpm was imposed. The value has been chosen because the density of the methane is about one-third of the one of the oxygen and thus its pump requires either a high rotation speed or multiple stages to achieve its scope.

The input conditions for the design of the turbopump in this paper are as follows:

- For the oxygen pump the conditions are as follows:

- Total pressure at inlet: 4.3 bar;
- Temperature of the oxygen: 90 K;
- Mass flow of the oxygen: 6.581 kg/s;
- Outlet pressure: 90 bar.

- For the methane pump the conditions are as follows:
  - Total pressure at inlet: 4.3 bar;
  - Temperature of the methane: 115 K;
  - Mass flow of the methane: 1.955 kg/s;
  - Outlet pressure: 130 bar.
- For the turbine the conditions are as follows:
  - Working fluid: supercritical methane;
  - Total pressure at inlet: 120 bar;
  - Total temperature at inlet: 600 K;
  - Mass flow of the methane: 1.955 kg/s.

2.2. Turbopump Architecture Determination

Following the establishing of the input conditions, a trade-off of different arrangement solutions has been carried out.

The first design solution is presented in Figure 1. oxygen and methane pumps have same orientation, while the turbine is back-to-back with the methane pump.

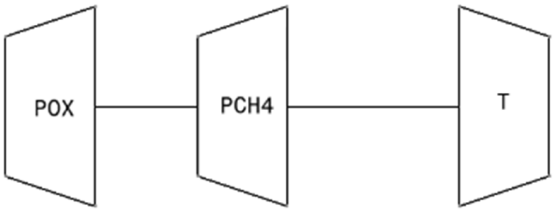

Figure 1. First design solution for the arrangement solution.

The second design solution is presented in Figure 2. oxygen and methane pumps have an inlet-to-inlet orientation, while the turbine is back-to-back with the methane pump.

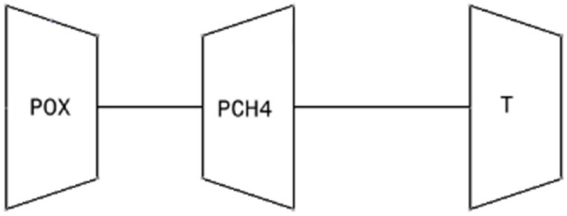

Figure 2. Second design solution for the arrangement solution.

Figures 1 and 2 depict the two arrangements considered.

The advantages of the first solution are as follows:

- It is simpler than the second solution;
- The end-shaft pump (in this case the POX) has a higher level of available NPSH;
- The end-shaft pump (in this case the POX) has better efficiency.

The disadvantages of the first solution are as follows:

- The load on the bearings is higher due to the fact that the axial forces induced by the pumps will add up;
- The sealing system required is more complex;
- The risk of explosion is higher.

The advantages of the second solution are as follows:

- The axial forces in the pump are minimized due to the opposing direction of pump positioning;
- A reduction in the pressure difference between the adjacent components by up to 9 times;
- A reduction in complexity of the sealing system;
- A reduction in stress on the bearings.

The disadvantages of the second solution are as follows:

- The POX requires a volute, which translates to an added complexity to the system;
- The available NPSH of the POX is lower as a consequence of adding the volute;
- The efficiency of the POX is lowered due to losses in the inlet volute (a loss of about 0.35% is expected in the case of the present design).

While the arrangement solution in Figure 1 is used in the single-shaft turbopump assemblies in existence, the one in Figure 2 is a novel solution.

After considering the advantages and disadvantages of each of the presented configurations, it has been decided that the best design solution for this application is the second solution.

2.3. Preliminary Geometry Creation

The preliminary geometry of the pumps and the turbine has been created using the CFturbo software (CFturbo 2024 R1.2) suite [11].

This software suite creates models of rotating machines based on input from users.

The pumps and the turbine were segregated and treated independently.

Figures 3–5 present the CFturbo 3D view of the turbopump components. The empty space between the impeller and the outlet volute of the methane pump is intentional and it was filled in the CFD analysis and the mechanical design.

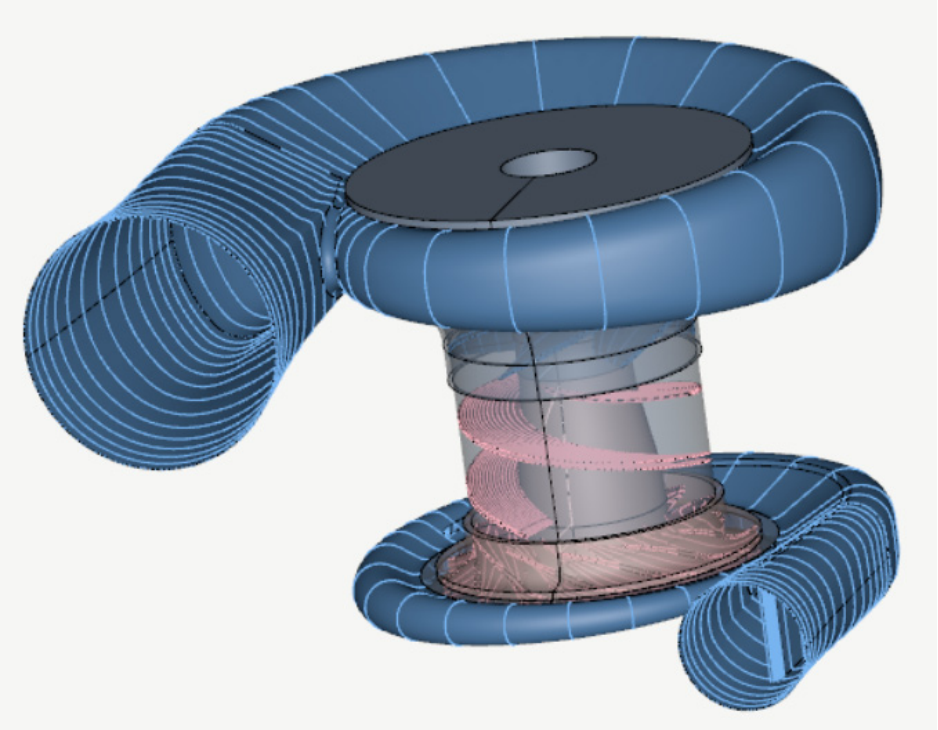

Figure 3. Oxygen pump 3D view (CFturbo).

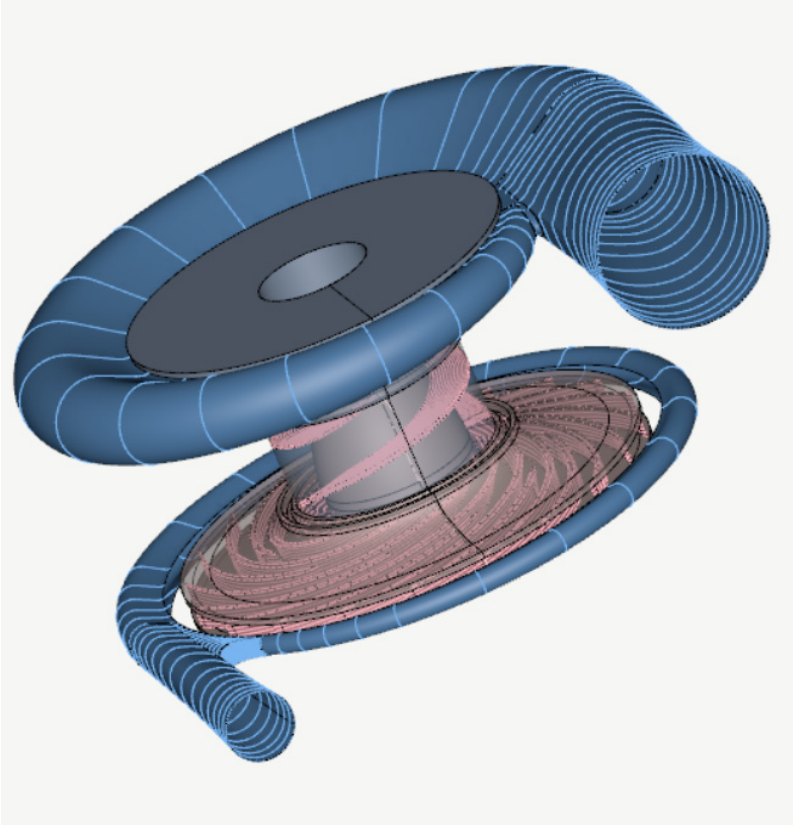

Figure 4. Methane pump 3D view (CFturbo).

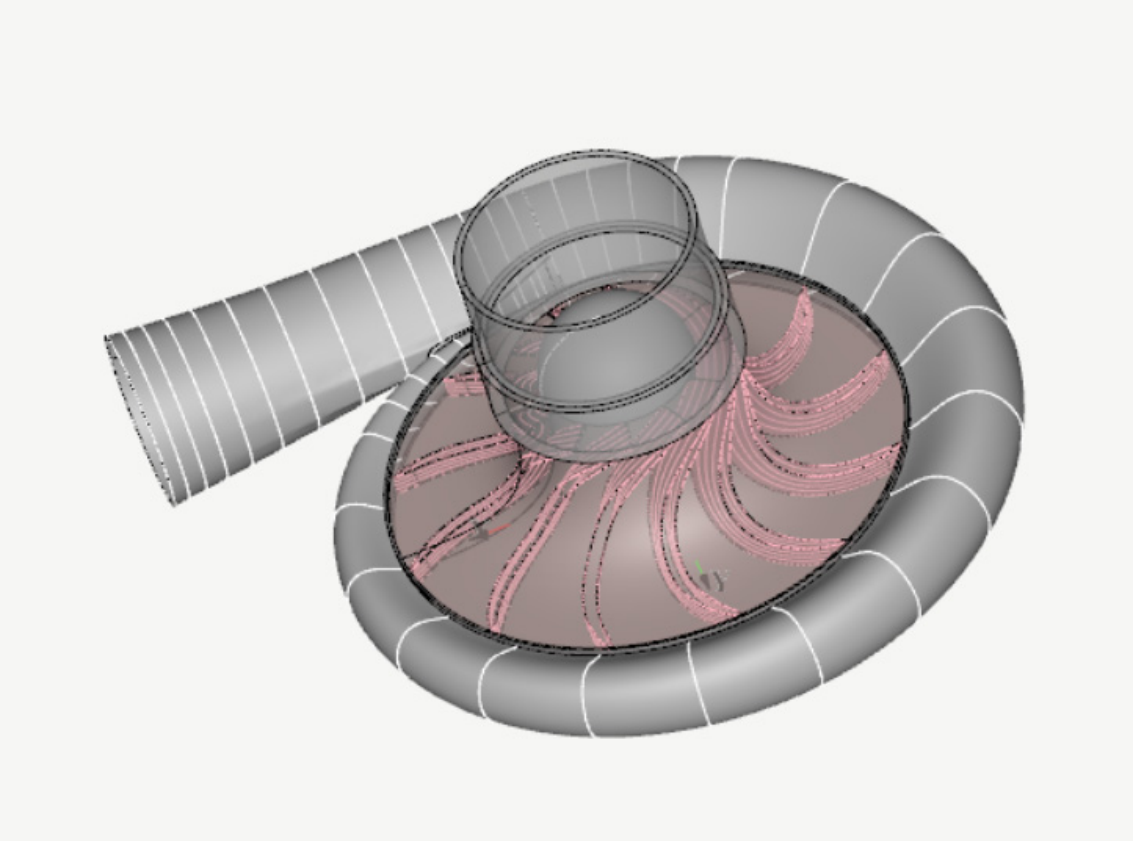

Figure 5. Turbine 3D view (CFturbo).

The oxygen pump is composed of an inlet volute designed using the Pfleiderer design rule which applies the principle of momentum conservation [12]. Its dimensions have been chosen such that the flow is as slow as possible (taking also into account dimension restrictions).

The volute is followed by a 6-blade radial-to-axial deviation stator, which has the role of guiding the flow of oxygen and providing an axial inflow in the inducer.

The inducer has 2 blades and has the scope to eliminate the possibility of cavitation appearance in the impeller.

The impeller has 12 blades and provides most of the pressure increase for the oxygen. Its outlet diameter has been defined using the Cordier Diagram [13].

Lastly, the outlet volute has been designed by using the Pfleiderer design rule. The impossibility of obtaining a correct flow using a simple volute imposed that a double volute shall be used instead.

The methane pump is composed of an inlet volute designed using the same reasoning as in the case of the oxygen inlet volute.

It is then followed by an 8-blade radial-to-axial deviation stator with the same role as the one of the oxygen.

The inducer has 2 blades.

The impeller has 10 main blades and 10 splitters. The choice to use splitters has been taken because the flow at the outlet indicated the need to increase the number of blades, but doing so with only main blades would lower too much of the area at the inlet, blocking the correct flow of the methane. The splitters fix this issue by the fact that they are shorter and their leading edge can be positioned in a location where they do not create further problems to the flow.

The outlet volute is a simple volute, created using the Pfleiderer design rule.

The turbine inlet volute was designed using the Pfleiderer rule, but the flow imposed that its shape to be changed to the one of a volute designed using the Stepanoff rule with a coefficient k_s of 0.9 [14].

The impeller has 12 blades. Its meridional shape has been designed taking into account that the change in the direction of the flow shall be as smooth as possible in order to eliminate the losses [15,16].

Table 1 presents the number of blades of each component's rotating parts.

Table 1. Components' number of blades.

Component	POX	PCH4	T
Inducer	2	2	-
Impeller	12	10 + 10 (splitters)	12

The wrap angle of all the bladed components has been defined having in mind to obtain a smooth direction change in the flow channels in order to avoid losses. Authors of paper [17] analyse the correlation between the wrap angle of the impeller blades and the hydraulic and mechanical performances of the pump impellers used in the study.

3. Design Justification

To verify the design of the turbine and the pumps, the geometries obtained in CFturbo have then been exported to an ANSYS Workbench system [18,19].

The meshing has been performed with ANSYS Mesher in the case of volutes and the outlet channel of the turbine.

The general settings for the mesh are as follows:

- Element size: 0.5 mm;
- Element order: quadratic;
- Inflation on all metal–fluid interfaces.

- First-layer thickness: 0.05 mm;
- Number of layers: 5;
- Growth rate: 1.2.

In the case of bladed components (bladed stators, inducers and impellers), a mesh has been created using ANSYS Turbogrid.

The general settings for the mesh created with Turbogrid are as follows:

- Boundary Layer Refinement:
  - First element offset method: offset Y+ = 1;
  - Target expansion ratio: 1.2.
- Spanwise Blade Distribution Parameters:
  - Method: element count and size;
  - The number of elements and of constant elements is defined for each component individually to obtain the best possible mesh.

The mesh obtained using Turbogrid has been loaded in ANSYS ICEM and multiplied to obtain the whole circumference of the respective component.

The solver is ANSYS CFX. Each component was simulated independently. The main setup choices are as follows.

In the case of pumps:

- Reference pressure: 4.3 bar;
- Model fluid: isothermal with a fluid temperature set at 90 K in the case of the LOX pump and 115 K in the case of the LCH4 pump;
- Turbulence model: SST;
- All walls are non-slip with a roughness of 1.6 μm, with the exception of outlet volutes which have a roughness of 6.3 μm;
- Stator–Rotor interface model: Frozen Rotor;
- Stator–Stator and Rotor–Rotor interface model: None;
- Inlet boundary condition: subsonic flow regime with a mass and momentum option of total pressure (stable). The relative pressure: 0 bar;
- Outlet boundary condition: subsonic flow regime with a mass and momentum option of the mass flow rate. The mass flow rate is 6.581 kg/s in the case of the LOX pump and 1.955 kg/s in the case of the LCH4 pump and the mass flow area as specified.

In the case of the turbine:

- Reference pressure: 120 bar;
- Flow regime: subsonic;
- Heat transfer: total energy, with viscous work term included;
- Turbulence model: SST;
- All walls are non-slip with a roughness of 1.6 μm;
- Stator–Rotor interface model: Frozen Rotor;
- Inlet boundary condition: subsonic flow regime with a mass and momentum option of total pressure (stable). The relative pressure: 0 bar; the heat transfer option is total temperature: 600 K;
- Outlet boundary condition: subsonic flow regime with a mass and momentum option of the mass flow rate. The mass flow rate is 1.955 kg/s and the mass flow rate area is as specified.

After the analysis has been completed for a design, the results have been analyzed and changes have been made to it to fix the discovered issues.

In the case of the pumps, the following aspects have been considered for the optimization:

- Cavitation reduction or elimination.

The inlet angles and shape of the leading edge have been adapted to reduce the separation of the flow from the blade and reduce the cavitation.

- Elimination of flow separations or vortices.

The shape of the blades and their wrap angles and the shapes of the volutes (and especially of their cutwater) have been modified as needed to guarantee the correct flow and elimination of the flow separation zones.

- Outlet pressure.

The angles at the trailing edge of the pump impellers have been adapted to guarantee the flow deviation needed to obtain the required output pressure.

In the case of the turbine the following aspects have been considered for the optimization:

- Flow uniformity at the inlet in the impeller.

The volute shape has been updated until the best possible flow at the inlet in the impeller has been obtained. The bladed diffuser has been eliminated as result of this optimization.

- Elimination of flow separations or vortices.

The meridional shape and the shape of the blades has been adapted to eliminate the flow separation.

- Output power.

The blades' wrap angle and the angle at the trailing edge have been adapted until the required output power has been achieved.

4. Results and Discussion

In this chapter, the mechanical design of the turbopump and the results of the CFD analysis of each component are described.

The total pressure graphs are relative to the reference pressure.

4.1. Mechanical Design

The mechanical design of the turbopump is visible in Figure 6 [20].

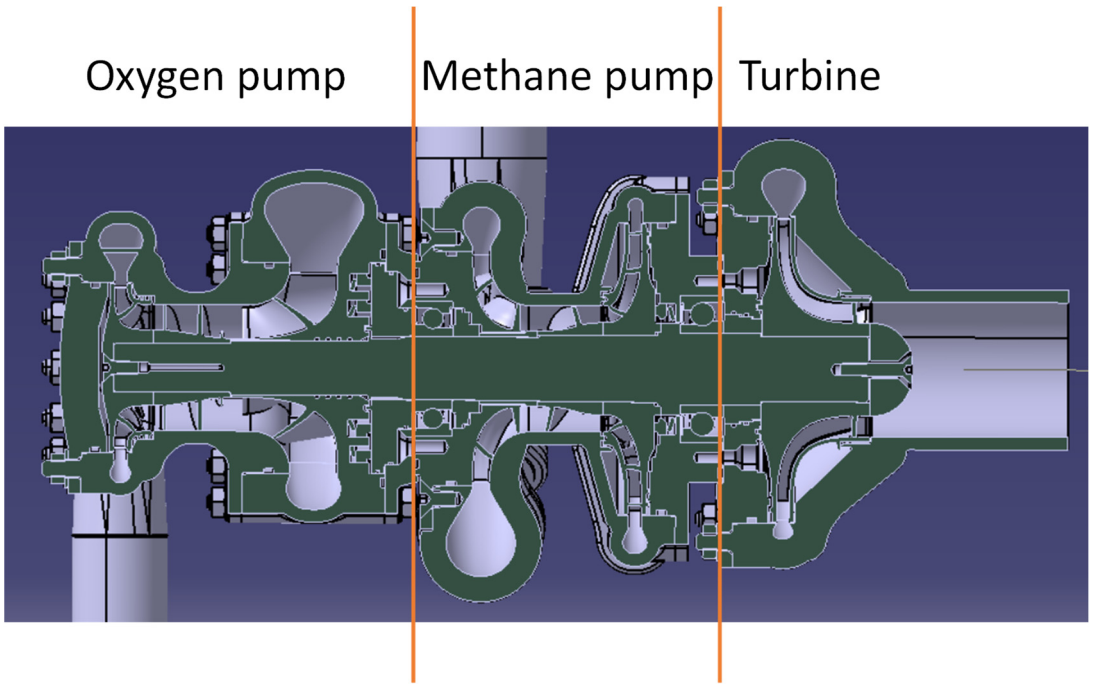

Figure 6. Cross-section through the single-shaft turbopump.

When comparing the absolute pressure graph of both pumps at the inlet of the inducer it can be observed that at the hub the values differ by less than 1 bar. This is relevant because in these zones there are openings created by the interstices between the rotating components and the static components of the single-shaft turbopump. As it can be seen in

the mechanical design, there is a communication path between these locations and, because of the low difference in pressure, the pressure-fed leakage is not favored, making it simple to seal this path.

The sealing path between the two pumps includes the following:

- A labyrinth seal on the path that passes through the middle of the oxygen pump inlet volute [21].

This labyrinth seal has the scope to reduce the pressure in the oxygen below the cavitation pressure.

- A floating ring seal.

This seal has the scope to close the leakage path. Both the seal and the surface on which it slides will be made of or covered by oxides of a high hardness to avoid their ignition during functioning. The floating ring seal has also the function to seal the leakage path when the turbopump is not working.

- A backup floating ring seal.

Taking into account that this leakage path is critical for the safe operation of the turbopump, a backup floating ring seal has been added. This has the scope to seal any accidental leakage from the first seal.

- A ball bearing with a double non-contact seal filled with grease.

Although the ball bearing is not taken into account to be used as a sealing method, it is mentioned in this category because at the nominal rotational speed of the pump the balls push the grease towards exterior and it will work as sealant. Supplementary grease will also be placed in the surrounding gaps for increased effect. The grease is of a special, oxygen compatible type.

Considering that liquids are prone to wash away the grease, measures have been taken to make them boil before entering into contact with it. The ball bearing is of type 7002 and can maintain the nominal rotation of the turbopump with grease lubrication.

- A stepped labyrinth seal on the path that passes through the middle of the methane pump inlet volute.

This labyrinth seal has the scope to lower the pressure of the methane below the cavitation point.

The sealing path between the methane pump and the turbine include the following:

- Teeth that force the liquid to change direction on the back side of the methane pump impeller.

These teeth have the scope to reduce the pressure of the methane.

- A floating ring seal.

This seal has the scope to close the seal path between the methane pump and the turbine. It works also as a static seal during the times when the pumps are not working.

- A ball bearing with a double non-contact seal filled with grease.

The ball bearing works in the same way as the one between the pumps. Its type is 7003 and it is also capable of maintaining the nominal rotation of the turbopump with grease lubrication.

- A stepped labyrinth seal.

This seal has the scope to reduce the pressure of the gas leaking from the turbine impeller.

As mentioned, the two ball-bearing models are chosen having in mind their capability to maintain the nominal rotation speed of the turbopump while being grease-lubricated. The proximity of the ball bearing to the surfaces washed by the cryogenic liquids allows the removal of the heat through their support and its transfer to the fluids. Having in mind that the heat transfer area is small while the mass flow of cryogenic fluids is large, it can be

concluded that the heat input to the fluids via this path is small enough for its effect to be considered negligible.

4.2. Mesh Sensitivity Analysis

To assess the independence of the results from the mesh, analyses have been carried with different mesh densities for the turbine and for the oxygen pump.

The results for the turbine investigation are as follows:

The mesh independence analysis results in case of the turbine are presented in Table 2. In this test, the geometry used is the one before the last, and there were three tests: 1× (12.2 million nodes), 3× (34.6 million nodes) and 5× (58.4 million nodes). The error between them is less than 1% on all investigated parameters, which indicates that the different mesh densities have a marginal influence on the results for the turbine case. The time needed to perform these analyses varied from 2–3 days (1×) to more than a month (5×). Taking this into account, it was concluded that the 1× mesh should be used because it provides results with a good confidence while the computational time is reduced significantly.

Table 2. Mesh independence analysis for turbine.

Parameter / Mesh Density	Output Power [W]	Deviation [%]	Turbine Efficiency [%]	Deviation [%]	Mass Flow Rate [kg/s]	Deviation [%]
1×	112,609	0	81.21	0	1.9552	0
3×	113,232	0.55	81.41	0.25	1.9549	0.02
5×	113,187	0.51	81.48	0.34	1.9559	0.04

In the case of the pumps, a mesh independence analysis has been carried out only on the oxygen pump, having in mind that the pumps are very similar in design and the physics involved and the short time available for this analysis. The last design of the oxygen pump has been used in this analysis.

The mesh independence analysis results are presented in Table 3. In this case five tests have been carried out: 0.8× (5.6 million nodes), 1× (7.1 million nodes), 1.05× (7.5 million nodes, but spread differently between components), 1.25× (8.8 million nodes) and 1.5× (10.5 million nodes).

Table 3. Mesh independence analysis for the oxygen pump.

Parameter / Mesh Density	Input Power [W]	Deviation [%]	Head Rise [%]	Deviation [%]
0.8×	65,952.3	1.95	919.499	1.48
1×	67,266.8	0	933.332	0
1.05× *	67,398.7	0.2	937.957	0.49
1.25×	67,242.3	0.03	934.067	0.08
1.5×	67,211.3	0.08	934.235	0.1

* The number of cells is almost identical to the ones in the 1× case, but they are spread differently between the components.

The variation in the investigated parameters indicates that for the 0.8× mesh they differ by more than 1% compared to the other mesh densities. This is caused by the small number of nodes, indicating that the number of nodes should be preferably increased to increase the accuracy of the analysis. For all other mesh densities, the results variation is less than 1%. Due to this reason, we have concluded that the 1× mesh provides an accurate enough result to be considered as the choice mesh density.

4.3. Oxygen Pump

The LOX pump must increase the total pressure of the LOX to 90 bar. Its output is connected to the injection system used to inject the LOX into the combustion chamber of the thruster.

In Figure 7 the pressure contours at the inlet of the inducer of the LOX pump are presented. The absolute (static) pressure contours at the inlet of the inducer indicate that the LOX maintains its liquid state. The cavitation pressure is 0.9935 bar [22]. The negative values shown in the total pressure contour do not contain the reference pressure component of 4.3 bar. By adding this component, it can be observed that all values become positive. The variation in the absolute pressure is an indication of the upstream influence exerted by the inducer to the flow. The pressure is higher above the current position of the inducer blades' leading edges and lower in the rest of the circumference.

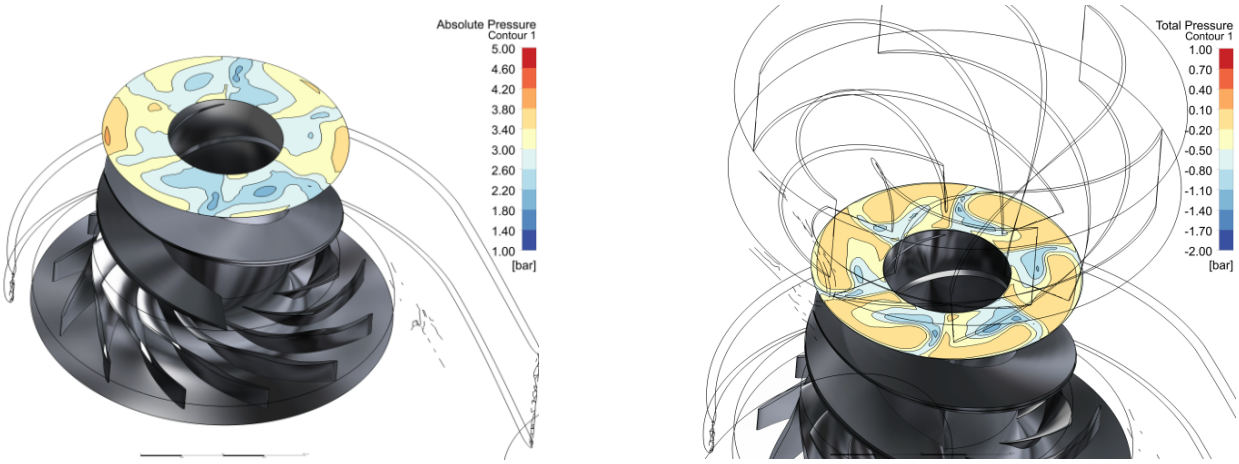

(**a**) (**b**)

Figure 7. Pressure contours at the inlet of the inducer of the LOX pump: (**a**) absolute (static) pressure, (**b**) total pressure.

The variation in the total pressure is an indication of the downstream influence of the inlet canalization blades. A low total pressure zone is observed on the suction side of the blades. The increase in total pressure from hub to shroud is not bad for the functioning the pump and actually helps in reducing the chance of cavitation appearing (and in the limitation of its intensity) because the fluid is accelerated more in the shroud zone compared to the hub zone.

The contour images in Figure 8 indicate that there are no problems with the flow and the fluid leaves the impeller uniformly and thus there is no flow-induced imbalance. The double volute was chosen as a solution due to issues discovered during previous design steps at the level of the cutwater of the volute, which were inducing an imbalance to the impeller that could only be solved this way.

The meridional plane pressure contours are presented in Figure 9. A low-pressure zone can be seen at the tip of the blades. This pressure is below the cavitation point and thus it indicates that cavitation occurs at the tip of the blades.

The locations where the pressure falls below the saturated vapour (cavitation) pressure are presented in Figure 10. There are two cavitation points located at the tip of the inducer blade. A second cavitation location is found in one of the channels of the impeller and on the leading edge of some of the blades.

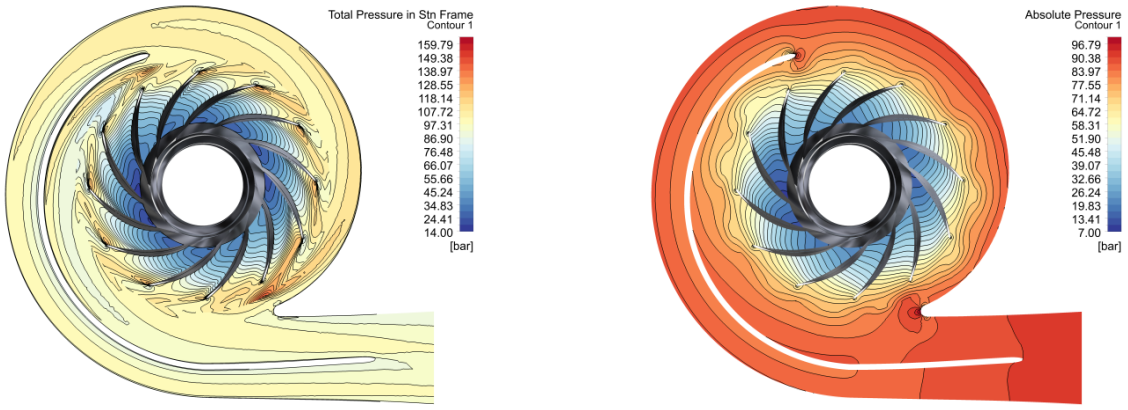

(**a**) (**b**)

Figure 8. Pressure contours in a plane that passes through the middle of the outlet from the impeller of the LOX pump: (**a**) total pressure in the stationary frame, (**b**) absolute (static) pressure.

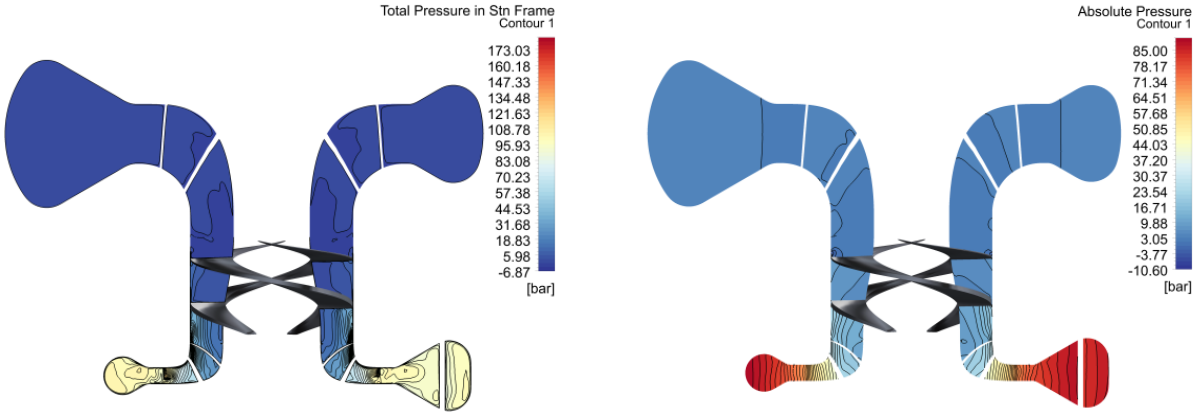

(**a**) (**b**)

Figure 9. Pressure contours in the meridional plane: (**a**) total pressure in the stationary frame, (**b**) absolute (static) pressure (inducer blades are made visible).

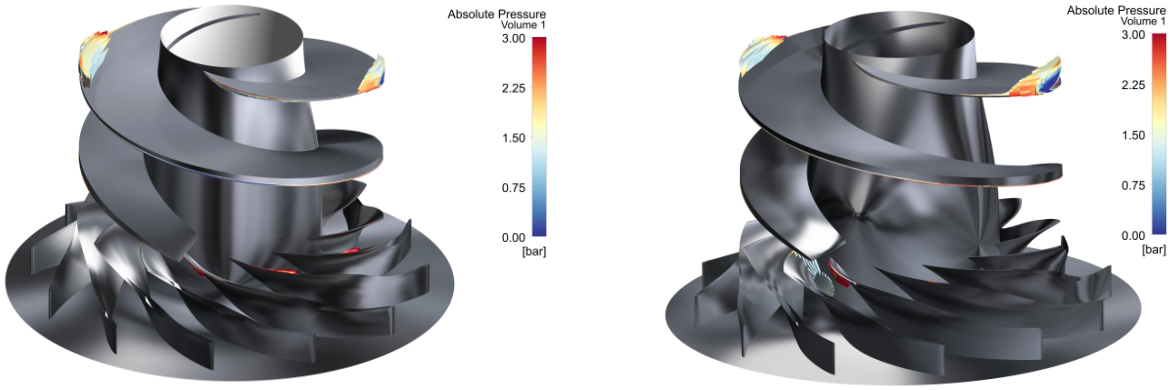

(**a**) (**b**)

Figure 10. Location of the low-pressure zones where pressure is below the cavitation pressure. The scale is limited on 0–3 bar: (**a**) front view, (**b**) back view.

Analysis of the evolution of low-pressure zones generated at the leading edge of the inducer blades reveals that they do not have a tendency to separate and migrate towards the impeller.

The pressure distribution at the outlet is presented in Figure 11. A variation in the LOX pressure is visible and is caused by the volute splitter.

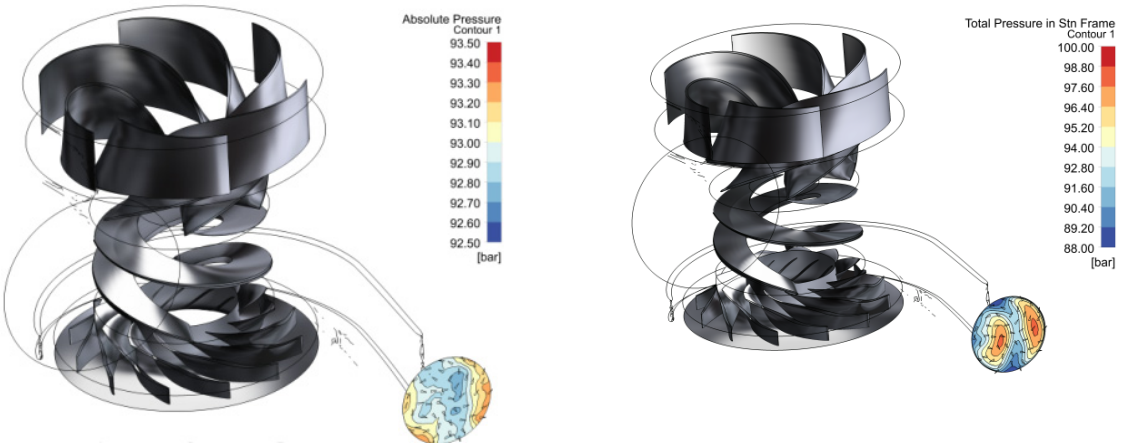

(**a**) (**b**)

Figure 11. Pressure distribution at the outlet: (**a**) absolute (static) pressure, (**b**) total pressure.

The variation is less than 1 bar in static pressure and less than 10 bar in total pressure.

The area averaged total pressure at the outlet of the pump is 98 bar. Reference pressure is also included in this value.

The efficiency of the pump is 76.3%.

The velocity streamlines, visible in Figure 12, indicate that there are no major flow separation zones, which could affect the efficiency of the pump.

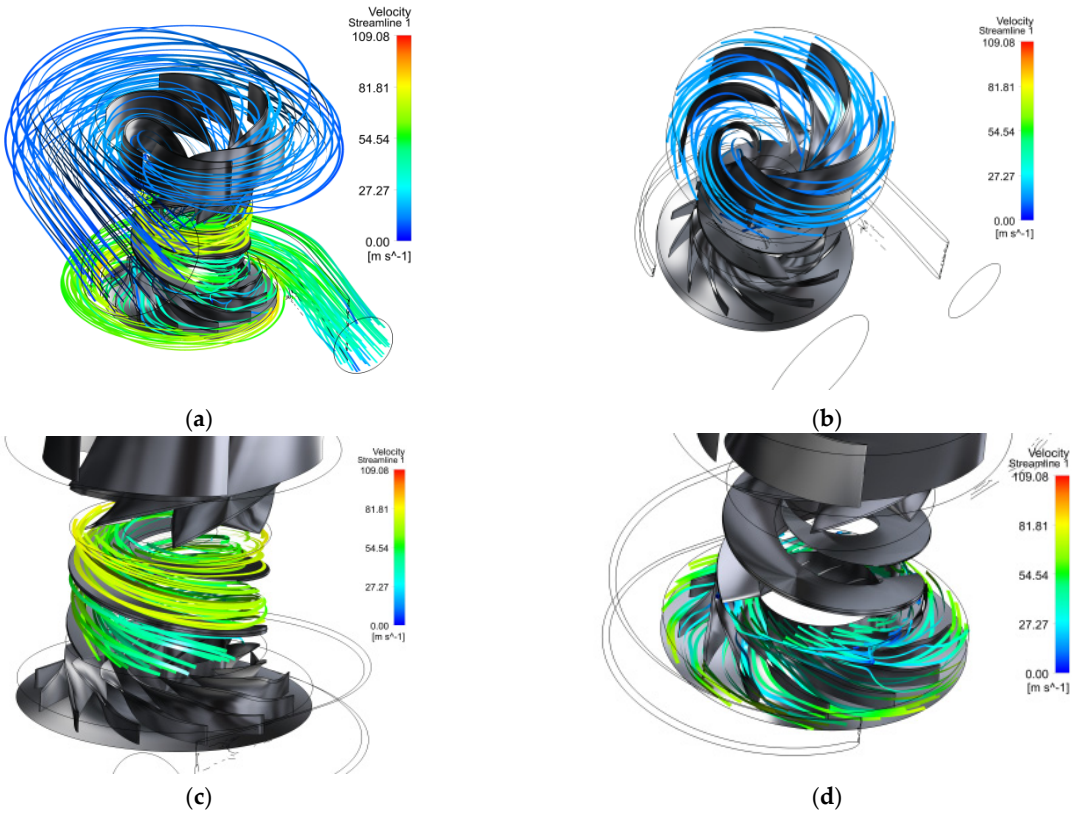

(**a**) (**b**)

(**c**) (**d**)

Figure 12. Velocity streamlines of the fluid passing through the LOX pump: (**a**) overview, (**b**) deviation stator, (**c**) inducer and (**d**) impeller.

4.4. Methane Pump

The LCH4 pump must increase the total pressure of the LCH4 to 130 bar. Its output is connected to the cooling channels of the nozzles where it will absorb energy from the hot walls, cooling them down.

The pressure contours at the inlet of the inducer of the LCH4 pump are presented in Figure 13. The absolute (static) pressure contours at the inlet of the inducer indicate that the LCH4 cavitation pressure (1.3221 bar [22]) is not achieved. The values shown in the total pressure contour are negative because they do not contain the reference pressure component of 4.3 bar. Taking into account that there is no location with a relative total pressure below −1 bar, it can be concluded that the absolute total pressure is above 3.3 bar.

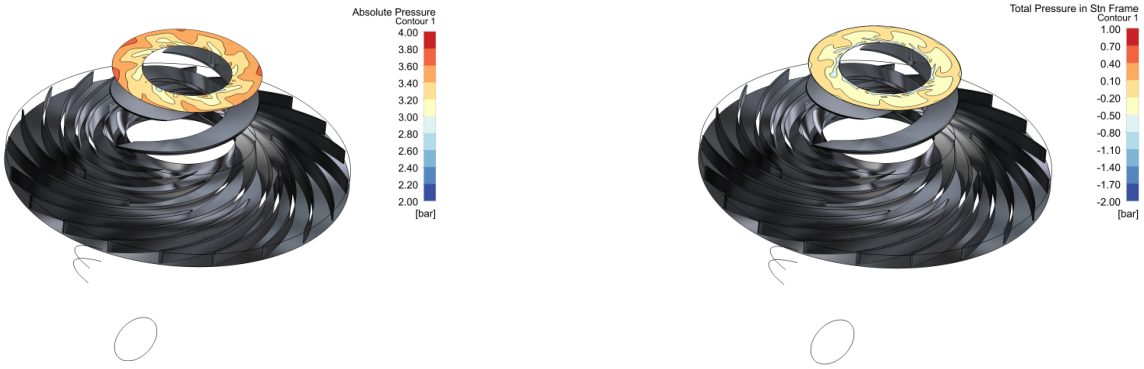

(**a**) (**b**)

Figure 13. Pressure contours at the inlet of the inducer of the LCH4 pump: (**a**) absolute (static) pressure, (**b**) total pressure.

The pressure lost in the inlet volute and stator is 0.25 bar, which is equivalent to an increase by 0.2% of the power required to obtain the same pressure at the outlet as in the situation where the admission would be carried out through an inlet pipe.

The pressure closer to the shroud is higher than the one closer to the hub. This variation is good for the cavitation behavior of the inducer.

In Figure 14 are presented the pressure contours on the symmetry plane of the outlet volute of the LCH4 pump. This plane also passes through the middle of the outlet from the impeller of the LCH4 pump, providing upstream information for the flow in the outlet volute. No indication of imbalance along the circumference of the impeller is present. In the diffuser of the outlet volute the liquid has the tendency to move slightly diagonally. This has, however, no visible impact on the pump performance.

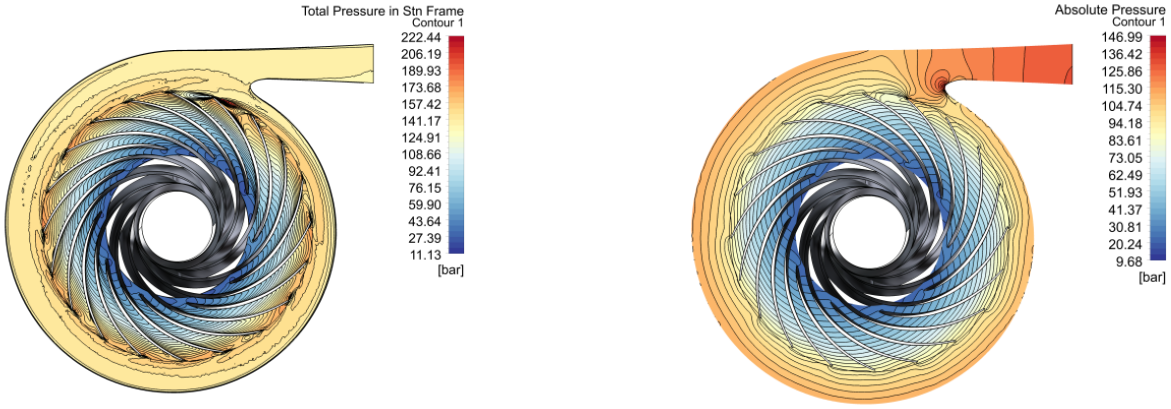

(**a**) (**b**)

Figure 14. Pressure contours in a plane that passes through the middle of the outlet from the impeller of the LCH4 pump: (**a**) total pressure in the stationary frame, (**b**) absolute (static) pressure.

By analyzing the pressure contours in the meridional plane presented in Figure 15, it can be seen that the static pressure is increased gradually in the impeller, without variations along the span of the blade.

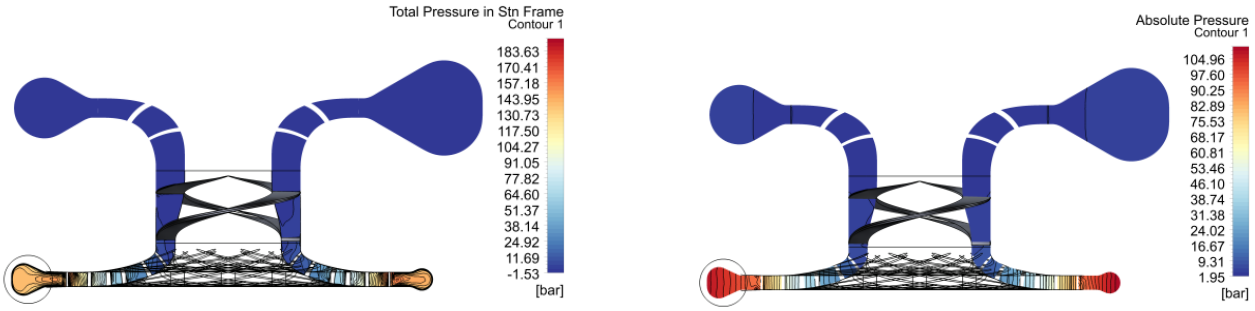

(**a**) (**b**)

Figure 15. Pressure contours in the meridional plane: (**a**) total pressure in the stationary frame, (**b**) absolute (static) pressure (inducer blades are made visible).

The locations where the pressure is below the cavitation pressure are presented in Figure 16. There are two cavitation points located on the suction side of the inducer blade. These two cavitation points are less than 1 mm in thickness and have a width of about 1.5 mm and cover the entire span of the blade.

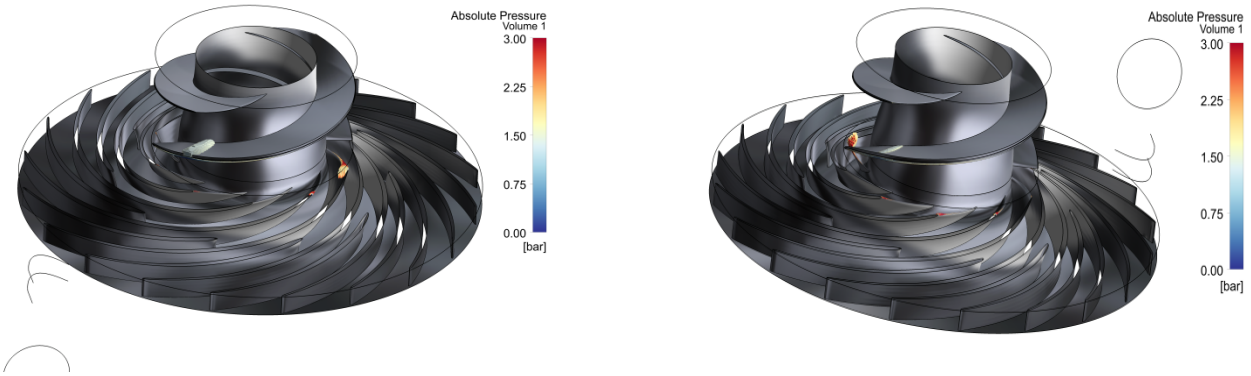

(**a**) (**b**)

Figure 16. Location of the low-pressure zones where pressure is below the cavitation pressure. The scale is limited on 0–3 bar: (**a**) front view, (**b**) back view.

A second cavitation location is found at the leading edge of the impeller blades, close to the shroud.

Analysis of their evolution does not indicate their tendency to grow and separate and migrate towards the impeller.

The pressure distribution at the outlet from the LCH4 pump is presented in Figure 17. A small variation in the methane pressure is observed along the surface of the outlet.

This variation is caused by the change in shape from the volute trapezoidal shape to the circular outlet volute diffuser.

It is less than 1.5 bar in static pressure and less than 15 bar in total pressure.

The area averaged total pressure, including the relative pressure value, at the outlet of the pump is 137.6 bar.

The efficiency of the pump is 70.6%.

The velocity streamlines in Figure 18 indicate that there are no major flow separation zones, which could affect the efficiency of the pump.

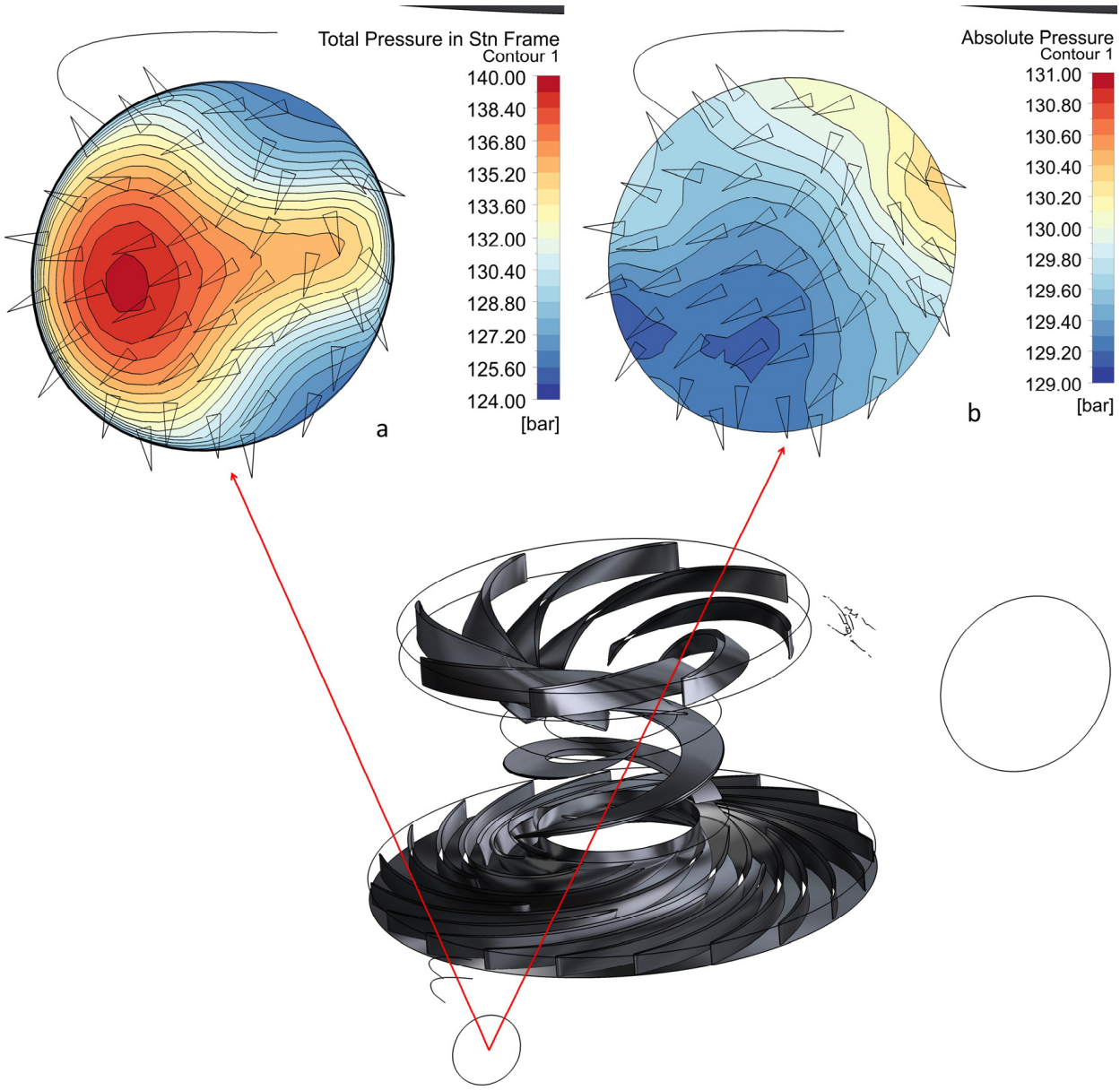

Figure 17. Pressure distribution at the outlet: (**a**) total pressure, (**b**) absolute (static) pressure.

4.5. Turbine

The turbine collects the fluid from the cooling channels of the nozzle and extracts a part of its energy and transforms it into mechanical energy which is needed to power the pumps. A total pressure loss of 10 bar is expected in the cooling channels.

Its output is connected to the injection system used to inject the LCH4 into the combustion chamber of the thruster.

The pressure contours at the inlet of the impeller of the turbine are presented in Figure 19. The absolute (static) pressure contours at the inlet of the impeller indicate that the LH2 is in supercritical condition. The absolute pressure contours indicate that the pressure is almost constant along the circumference of the impeller, with a notable difference appearing at the volute cutwater. This variation seems to be influenced by the position of the impeller blades with respect to the volute cutwater.

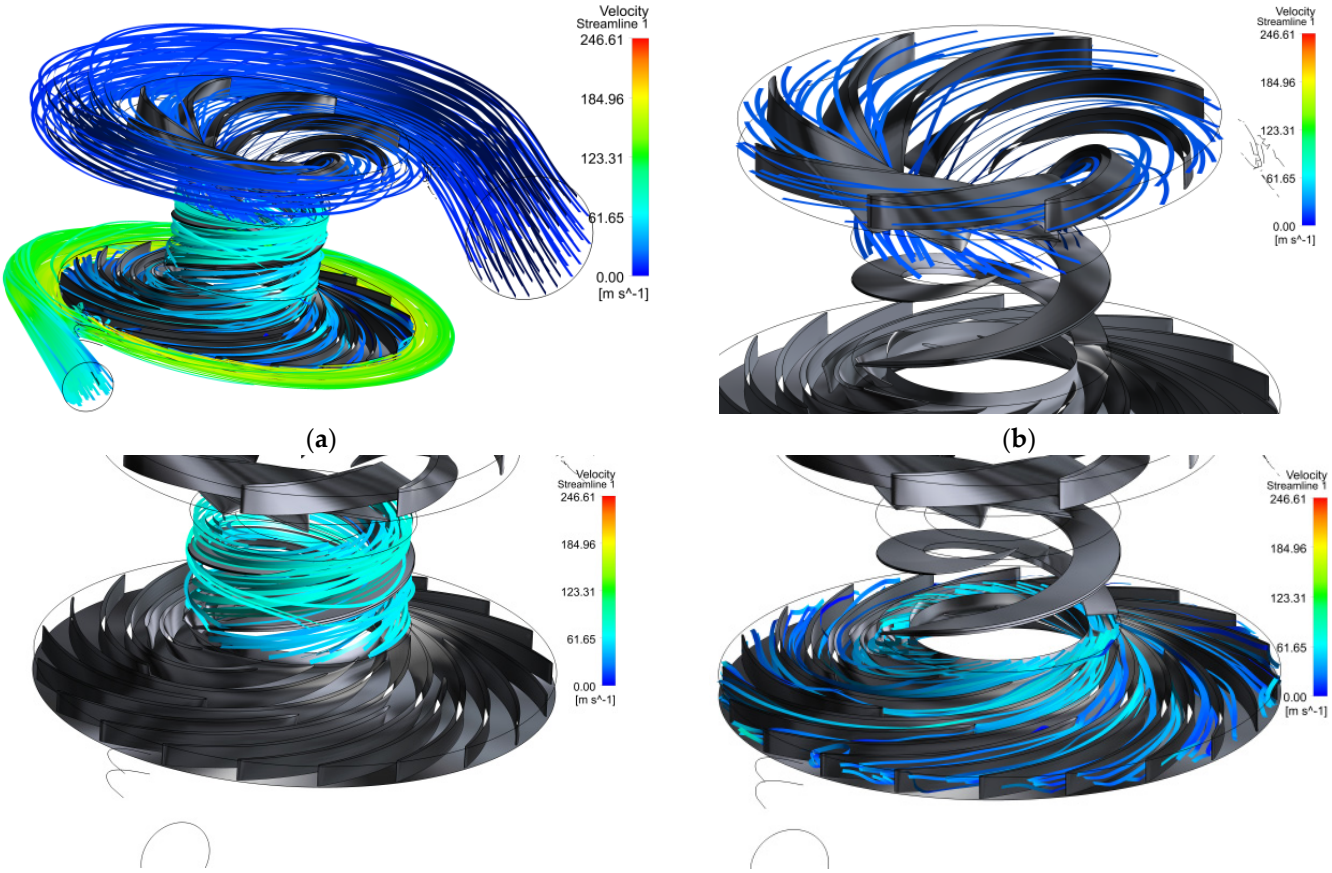

Figure 18. Velocity streamlines: (**a**) overview, (**b**) deviation stator, (**c**) inducer and (**d**) impeller.

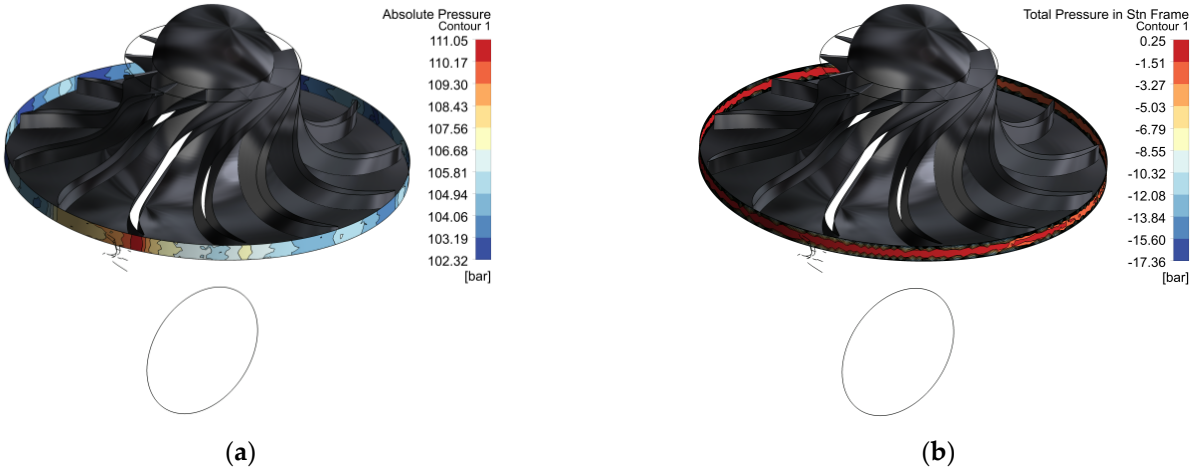

Figure 19. Pressure contours at the inlet of the impeller of the turbine: (**a**) absolute (static) pressure, (**b**) total pressure in the stationary frame.

The total pressure in the stationary frame contour indicates a variation in this parameter along the width of the impeller. The total pressure starts from a small value near the walls and grows up to the maximum value. This is normal and is caused by the boundary layer influence on the flow velocity. The total pressure is quasi-uniform along the circumference. The values shown in the total pressure contour are negative because they do not contain the reference pressure component of 120 bar.

The total pressure lost in the inlet volute is 1.44 bar.

The contour images in Figure 20 show the effect of the volute cutwater. At the passing of the blades in front of the cutwater, a small flow separation appears at their leading edge on the pressure side. This separation starts forming at an angle of about 15–20° before the pass and it reattaches immediately after. The separation appears in the plots as an increase in the total pressure plot and a decrease in the absolute pressure one. The reference pressure in the case of the total pressure plot is 120 bar.

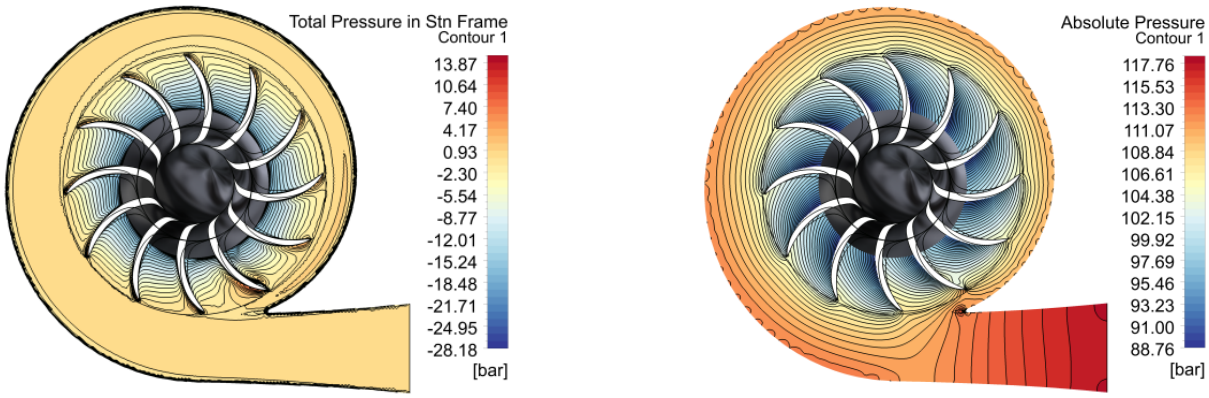

(**a**) (**b**)

Figure 20. Pressure contours in a plane that passes through the middle of the inlet volute of the turbine: (**a**) total pressure in the stationary frame, (**b**) absolute (static) pressure.

By analyzing the pressure contours in the meridional plane visible in Figure 21, it can be seen that the pressure decreases uniformly in the impeller. At the exit from the impeller, in the central zone of the outlet pipe, the pressure is much lower than the one closer to the walls. This is the result of the fact that the velocity at the outlet from the impeller is not axial and a vortex is formed. It was a design choice that allowed the increase in the power output of the turbine while maintaining the same dimensions. The increase in output power is 22%, with a loss in efficiency of 1%.

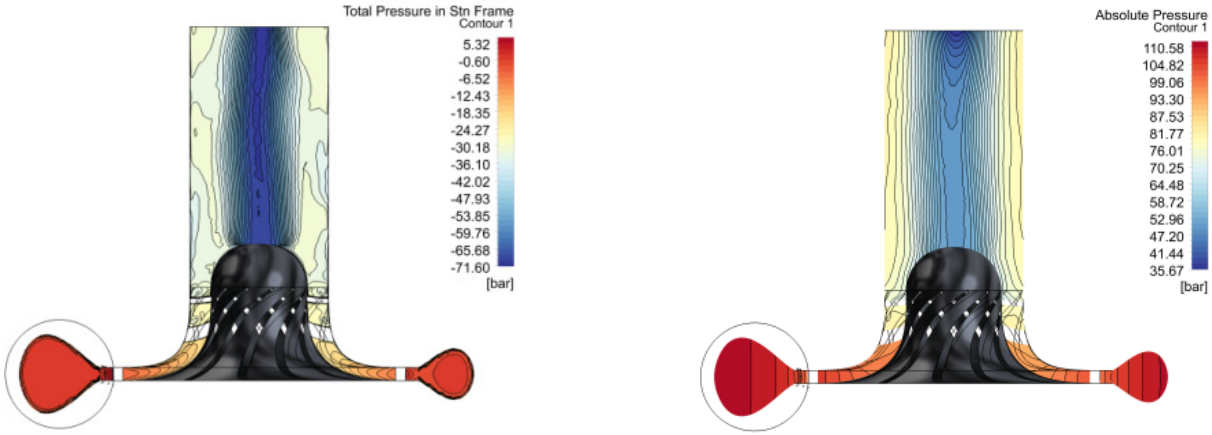

(**a**) (**b**)

Figure 21. Pressure contours in the meridional plane: (**a**) total pressure in the stationary frame, (**b**) absolute (static) pressure.

Figure 22 indicate that the pressure at the outlet decreases from the pipe surface to the middle. The arrows show the velocity direction, making clear the fact that, at the outlet, the fluid forms a vortex.

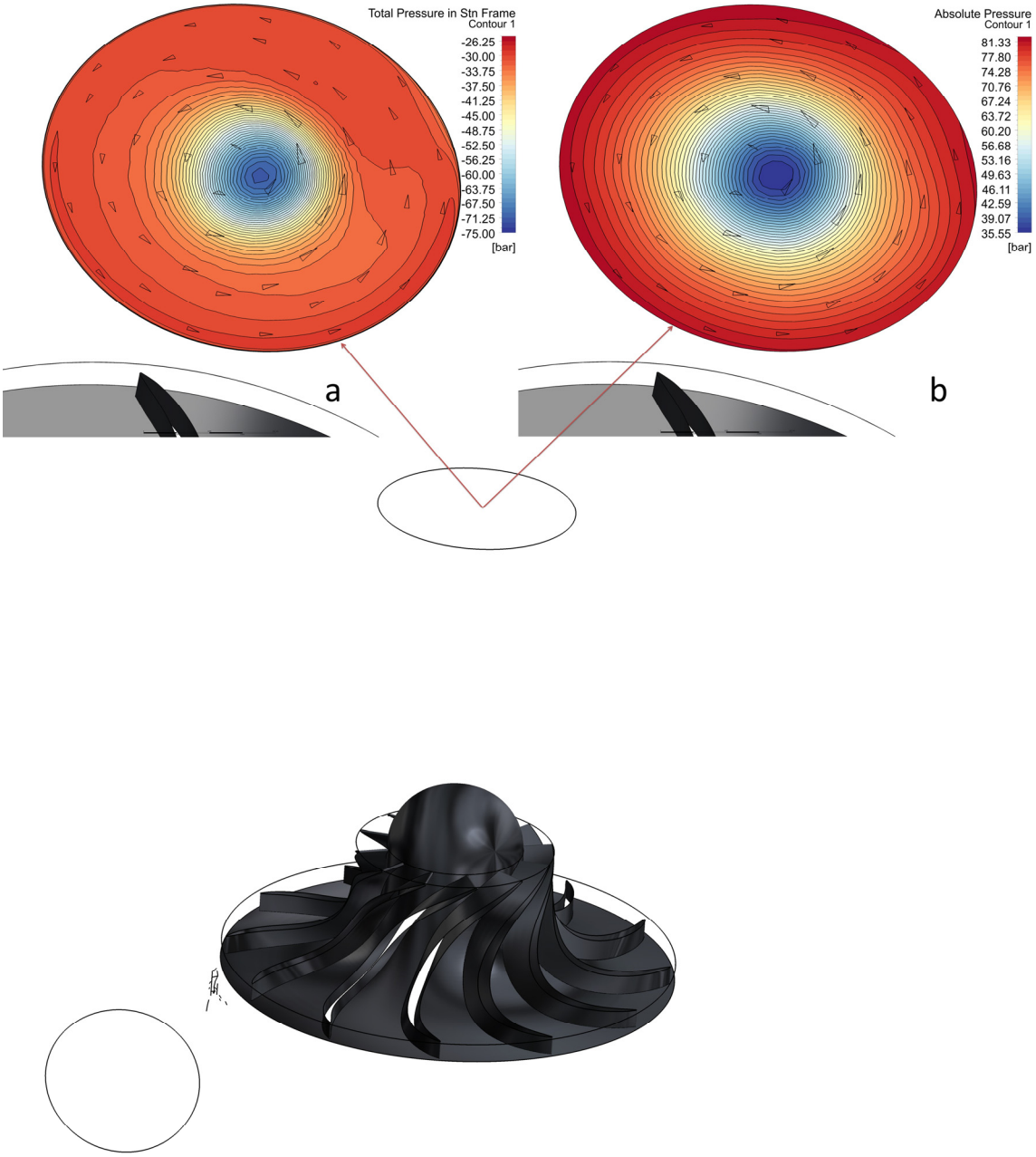

Figure 22. Pressure distribution at the outlet from the turbine: (**a**) total pressure, (**b**) absolute (static) pressure.

The area averaged total pressure, including the relative pressure value, at the outlet of the turbine is 84.2 bar.

The efficiency of the pump is 86.2%. The power output is 154.2 kW.

The velocity streamlines in Figure 23 indicate that there are no major flow separation zones, which could affect the efficiency of the pump. The vortex in the outlet pipe is visible.

By inspecting the velocity contours inside the impeller, visible in Figure 24, a clear tendency can be observed of the velocity increasing. The flow separation zone at the leading edge of the blade which is close to the inlet volute cutwater is visible as a darker, low-velocity zone. By looking at the blade that already passed the cutwater it can be seen that the separation zone has disappeared.

A way to limit this issue is to make the volute cutwater as close as possible to the impeller and make it as thin as possible. This solution has been taken into account; however,

it was found not to be feasible due to mechanical restrictions and it would induce a stress concentration point with possibly catastrophic implications.

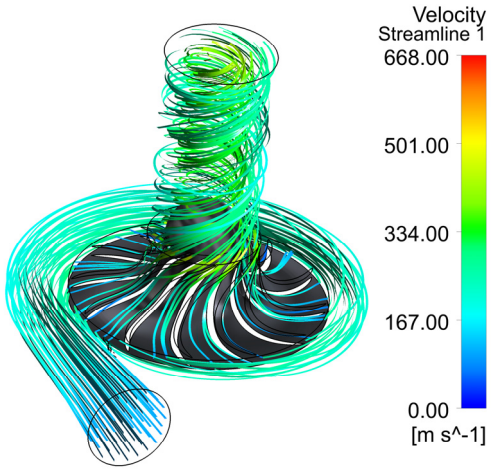

Figure 23. Velocity streamlines overview.

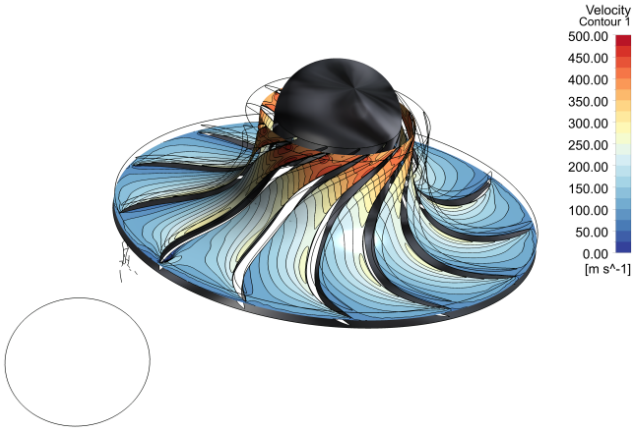

Figure 24. Velocity contours at 50% span inside the impeller.

The temperature contours in the meridional plane of the turbine is presented in Figure 25. The temperature decrease from the inlet volute to the outlet of the impeller can be clearly seen. This decrease is continuous and uniform, indicating that there are no issues in the evolution of the fluid inside the impeller.

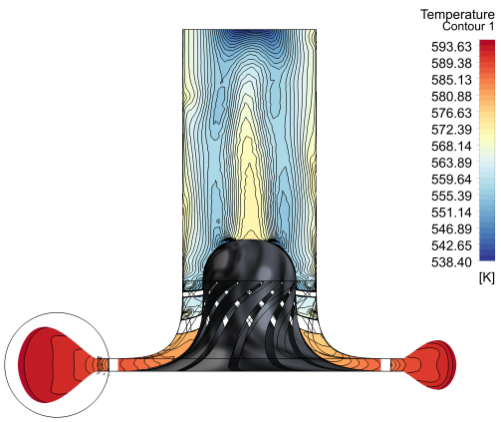

Figure 25. Temperature contours in the meridional plane.

In the outlet pipe, two zones of higher temperature are visible. These are caused by the viscous heating of the fluid and are a source of losses.

5. Future Work

The turbopump design presented in this paper has been accepted for manufacturing and is expected to be ready for testing in the second half of 2025.

The focus during the testing will be to verify the adequacy of the CFD analyses presented in this paper and to identify practical means of eliminating the cavitation. These include the following:

- The recovery of energy from secondary flows;
- Locally grinding the blade leading edge to lower the incidence angle.

A special attention will also be given to the sealing proper work. A previous testing campaign carried out on a model of the sealing indicated some issues that have been fixed in the present version.

6. Conclusions

The turbopump design proposed simplifies the thruster construction by eliminating the auxiliary systems of the turbopump while also keeping it at a very low weight.

As a direct result of implementing such a design, the reduction in costs is foreseen because it is simple and, also, has a small total weight.

The reserve of total pressure, calculated as the difference between the total pressure at the outlet from the pumps and the total pressure required by the engine, is 8 bar in the case of the oxygen pump and 7.6 bar in the case of the methane pump.

The secondary flow path from the back side of the LOX pump impeller is fully closed in this design compared to the classical way of arrangement of the pumps on a single-shaft turbopump; the total amount of LOX lost in the cavity behind the impeller is fixed and is limited to the volume of the cavity. Once it is filled no other oxygen will be able to enter it.

The turbine is capable of successfully powering the pumps and has a reserve power of 2 kW. Although this seems like a marginal reserve, one must consider all the other conservative estimations and contingencies.

Author Contributions: Conceptualization, A.-C.C.; Data curation, A.-M.T.A. and V.D.; Formal analysis, A.-C.C.; Investigation, A.-C.C.; Methodology, A.-C.C.; Supervision, D.-E.C.; Writing—original draft, A.-C.C.; Writing—review and editing, D.-E.C., S.-N.D. and V.D. All authors have read and agreed to the published version of the manuscript.

Funding: The input geometry for CFD analysis was carried with CFturbo software, which was made available free of charge to the authors.

Data Availability Statement: Dataset available on request from the authors.

Acknowledgments: The authors would like to thank the company CFturbo GmbH [10] for their kind approval of free usage of the software CFturbo.

Conflicts of Interest: The authors declare no conflicts of interest.

Abbreviations

LCH4	Liquid methane
LOX	Liquid oxygen
KBKhA	Chemical Automatics Design Bureau
RTGD	Radial Turbine Global Design
POX	Oxygen pump
PCH4	Methane pump
T	Turbine
NPSH	Net pressure suction head

References

1. Importance of Methane | US EPA. Available online: https://www.epa.gov/gmi/importance-methane (accessed on 5 August 2024).
2. Landspace Assembles Methalox Engine, Signs International Agreements—SpaceNews. Available online: https://spacenews.com/landspace-assembles-methalox-engine-signs-international-agreements/ (accessed on 5 August 2024).
3. Available online: https://www.blueorigin.com/engines/be-4 (accessed on 5 August 2024).
4. Available online: https://newspaceeconomy.ca/2024/04/15/spacexs-revolutionary-raptor-engine-powering-the-future-of-spaceflight/?amp=1 (accessed on 5 August 2024).
5. Available online: https://www.avio.com/it/m-10 (accessed on 5 August 2024).
6. Demyanenko, Y.; Dmitrenko, A.; Rachuk, V.; Shostak, A.; Minick, A.; Bracken, R.; Buser, M. Single-Shaft Turbopumps in Liquid Rocket Engines. In Proceedings of the 42nd AIAA/ASME/SAE/ASEE Joint Propulsion Conference & Exhibit, Sacramento, CA, USA, 9–12 July 2006.
7. Pempie, P.; Vernin, H. Multi Purposes Reusable LOX/CH4 Bleed Rocket Engine. In Proceedings of the 7th European Conference for Aeronautics and Space Sciences (EUCASS), Milan, Italy, 3–6 July 2017.
8. Leto, A.; Bonfiglioli, A. Preliminary Design of a Radial Turbine for Methane Expander Rocket-Engine. In Proceedings of the 72nd Conference of the Italian Thermal Machines Engineering Association, ATI 2017, Lecce, Italy, 6–8 September 2017.
9. Andreescu, T.; Mangra, A.; Vilag, V.; Mălăel, I.; Căncescu, A.; Vilag, J.; Ifrim, D.; Dănescu, S. LOX/LCH4 Upper Stage Development Strategies for Future Launchers. *TURBO* **2019**, *VI*, 15–26.
10. Sutton, G.P.; Biblarz, O. *Rocket Propulsion Elements*, 8th ed.; John Wiley & Sons: Hoboken, NJ, USA, 2011.
11. Available online: www.cfturbo.com (accessed on 5 August 2024).
12. Pfleiderer, C. *Die Kreiselpumpen*; Springer: Berlin/Heidelberg, Germany, 1924; ISBN 9783662431474.
13. Epple, P.; Durst, F.; Delgado, A. A theoretical derivation of the Cordier diagram for turbomachines. *Proc. Inst. Mech. Eng. Part C J. Mech. Eng. Sci.* **2010**, *225*, 354–368. [CrossRef]
14. Stepanoff, A.J.; Medalist, M. *Ingersoll-Rand (Company). Centrifugal and Axial Flow Pumps Theory, Design, and Application*, 2nd ed.; John Wiley & Sons, Inc.: New York, NY, USA, 1957; ISBN 0-89464-723-7.
15. Barbarelli, S.; Amelio, M.; Florio, G. Predictive model estimating the performances of centrifugal pumps used as turbines. *Energy* **2016**, *107*, 103–121. [CrossRef]
16. Gunawan, G.; Pemana, D.I.; Sutikno, P. Design and numerical simulation of radial inflow turbine of the regenerative Brayton cycle using supercritical carbon dioxide. *Results Eng.* **2023**, *17*, 100931. [CrossRef]
17. Tan, L.; Zhu, B.; Cao, S.; Bing, H.; Wang, Y. Influence of Blade Wrap Angle on Centrifugal Pump Performance by Numerical and Experimental Study. *Chin. J. Mech. Eng.* **2014**, *27*, 171–177. [CrossRef]
18. Lipej. Challenges in the Numerical Analysis of Centrifugal Pumps: Energetic, Cavitation and Dynamic Characteristics. *Eng. Technol. Appl. Sci. Res.* **2022**, *12*, 8217–8222. [CrossRef]
19. Mirdrikvand, M.; Roozbehani, B.; Moqadam, S.I.; Roshan, A.C.; Ramezani, Y. Velocity Boundary Layer Analysis of a Flat Plate Heat Exchanger in Laminar Flow: A Case Study. *Eng. Technol. Appl. Sci. Res.* **2012**, *2*, 310–314. [CrossRef]
20. Gülich, D.-I.; Johann, F. *Kreiselpumpen: Ein Handbuch für Entwicklung, Anlagenplanung und Betrieb*; Springer: Berlin/Heidelberg, Germany, 1999; ISBN 3540569871/9783540569879.
21. Eldin, A.M.G. Leakage and Rotordynamic Effects of Pocket Damper and See-through Labyrinth Seals. Ph.D. Thesis, Office of Graduate Studies of Texas A&M University, College Station, TX, USA, 2007.
22. Linstrom, P.J.; Mallard, W.G. *NIST Chemistry WebBook, NIST Standard Reference Database Number 69*; National Institute of Standards and Testing (NIST): Gaithersburg, MD, USA, 2013. [CrossRef]